Kondo effect in an integer-spin quantum dot

S. Sasaki*, S. De Franceschi†, J. M. Elzerman†, W. G. van der Wiel†, M. Eto†‡, S. Tarucha*§ & L. P. Kouwenhoven†

* *NTT Basic Research Laboratories, Atsugi-shi, Kanagawa 243-0129, Japan*
† *Department of Applied Physics, DIMES, and ERATO Mesoscopic Correlation Project, Delft University of Technology, PO Box 5046, 2600 GA Delft, The Netherlands*
‡ *Faculty of Science and Technology, Keio University, 3-14-1 Hiyoshi, Kohoku-ku, Yokohama 223-8522, Japan*
§ *ERATO Mesoscopic Correlation Project, University of Tokyo, Bunkyo-ku, Tokyo 113-0033, Japan*

The Kondo effect—a many-body phenomenon in condensed-matter physics involving the interaction between a localized spin and free electrons—was discovered in metals containing small amounts of magnetic impurities, although it is now recognized to be of fundamental importance in a wide class of correlated electron systems[1,2]. In fabricated structures, the control of single, localized spins is of technological relevance for nanoscale electronics[3,4]. Experiments have already demonstrated artificial realizations of isolated magnetic impurities at metallic surfaces[5,6], nanoscale magnets[7], controlled transitions between two-electron singlet and triplet states[8], and a tunable Kondo effect in semiconductor quantum dots[9–12]. Here we report an unexpected Kondo effect in a few-electron quantum dot containing singlet and triplet spin states, whose energy difference can be tuned with a magnetic field. We observe the effect for an even number of electrons, when the singlet and triplet states are degenerate. The characteristic energy scale is much larger than in the ordinary spin-1/2 case.

Quantum dots are small electronic devices[13], which confine a well-defined number of electrons, N. The total spin is zero or an integer for even N, and half-integer for odd N. The latter case is the canonical example of the Kondo effect[14,15] when all electrons can be ignored, except for the one with the highest energy; that is, the case of a single, isolated spin, $S = 1/2$ (Fig. 1a). Although the energy level of the electron ϵ_o is well below the Fermi energies of the two leads, Heisenberg uncertainty allows the electron on the dot to tunnel to one of the leads whereupon it is replaced quickly by another electron. The timescale for such a co-tunnelling process[16] is $\sim\hbar/U$, where $h = 2\pi\hbar$ is Planck's constant and U is the on-site Coulomb energy. Figure 1a illustrates that particle exchange by co-tunnelling can effectively flip the spin on the dot. At low temperature, the coherent superposition of all possible co-tunnelling processes involving spin flip can result in a time-averaged spin equal to zero. The whole system—that is, quantum dot plus electrodes—forms a spin singlet. The energy scale for this singlet state is the Kondo temperature, T_K. In terms of density of states, a narrow peak with a width $\sim k_B T_K$ develops at the Fermi energy (k_B is Boltzmann's constant). Note that for even N and $S = 0$, co-tunnelling gives rise to a lifetime broadening of the confined state, without producing any Kondo resonance. Such even/odd behaviour corresponding to no-Kondo/Kondo has been observed in recent experiments[9,10].

It is also possible that a quantum dot with even N has a total spin $S = 1$; for example, when the last two electrons have parallel spins. If the remaining $N - 2$ electrons can be ignored, this corresponds to a triplet state. Parallel spin filling is a consequence of Hund's rule occurring when the gain in exchange energy exceeds the spacing between single-particle states[8]. The spin of the triplet state can also be screened by co-tunnelling events. These are illustrated in the centre-left side of Fig. 1b. In contrast to single-particle states that are considered in the spin-1/2 Kondo problem, the spin triplet consists of three degenerate two-particle states. Co-tunnelling exchanges only one of the two electrons with an electron from the leads. The total spin of the many-body Kondo state depends on how many modes in the leads couple effectively to the dot[17,18]. If there is only one mode, the screening is not complete and the whole system does not reach a singlet state. In this case the Kondo effect is called "underscreened". Calculations show that also for $S = 1$ a narrow Kondo resonance arises at the Fermi energy, but the corresponding T_K is typically lower than in the case of $S = \frac{1}{2}$ (refs 19, 20). Some experiments have reported the absence of even/odd behaviour[21,22], which may be related to the formation of higher spin states.

Here we investigate a quantum dot with even N, where the last two electrons occupy a degenerate state consisting of a spin singlet and a spin triplet. Figure 1b illustrates the different co-tunnelling processes occurring in this special circumstance. Starting from $|S = 1, S_z = 1\rangle$, where S_z is the z-component of the total spin on the dot, co-tunnelling via a virtual state $|1/2,1/2\rangle$ can lead either to the triplet state $|1,0\rangle$ or to the singlet state $|0,0\rangle$. Via a second co-tunnelling event, the state $|1, -1\rangle$ can be reached. As for the $S = 1$ case, the local spin can fluctuate by co-tunnelling events. By

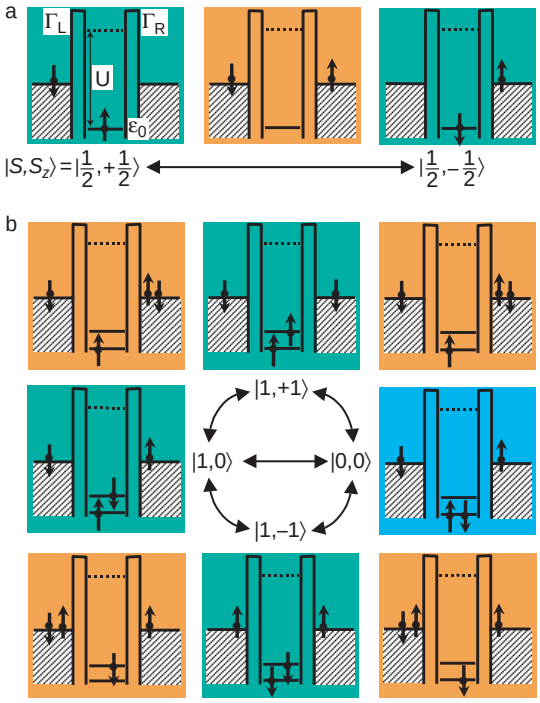

Figure 1 Spin-flip processes leading to ordinary and singlet–triplet Kondo effect in a quantum dot. **a**, Co-tunnelling event in a spin-1/2 quantum dot for odd N. Only the highest-energy electron is shown, occupying a single spin-degenerate level, ϵ_0. (The case of two, or more, closely spaced levels has also been considered theoretically within the context of the spin-1/2 Kondo effect[30].) The green panels refer to $S_z = 1/2$ and $-1/2$ ground states, which are coupled by a co-tunnelling event. The two tunnel barriers have tunnelling rates Γ_R and Γ_L. In the Coulomb blockade regime ($|\epsilon_0| \sim U$), adding or subtracting an electron from the dot implies an energy cost $\sim U$. Hence the intermediate step (orange panel) is a high-energy, virtual state. The spin-flip event depicted here is representative of a large number of higher-order processes which add up coherently such that the local spin is screened. This Kondo effect leads to an enhanced linear-response conductance at temperatures $T \ll T_K$. **b**, Co-tunnelling in an integer-spin quantum dot for even N at a singlet–triplet degeneracy. Two electrons can share the same orbital with opposite spins (singlet state in the blue panel) or occupy two distinct orbitals in one of the three spin-triplet configurations (green panels). The different spin states are coupled by virtual states (orange panels). As in the spin-1/2 case, spin-flip events can screen the local magnetic moment. Note that an $S = 1$ Kondo effect only involves $|1,+1\rangle$, $|1,0\rangle$ and $|1, -1\rangle$.

coupling to all triplet states, the singlet state enhances the spin exchange interaction between the dot and the leads, resulting in a higher rate for spin fluctuations. This particular situation yields a strong Kondo effect, which is characterized by an enhanced T_K. This type of Kondo effect has not been considered before, probably because a singlet–triplet degeneracy does not occur in magnetic elements. Recent scaling calculations by Eto and Nazarov indeed indicate a strong enhancement of T_K at the singlet–triplet degeneracy[23]; these workers also argue[23] that the total spin of the many-body Kondo state behaves as in the case of $S = 1$.

Our quantum dot has the external shape of a rectangular pillar (Fig. 2a, b) and an internal confinement potential close to a two-dimensional ellipse[24]. The tunnel barriers between the quantum dot and the source and drain electrodes are thinner than in our previous devices[8,24] such that co-tunnelling processes are enhanced. Figure 2d shows the linear response conductance (d.c. bias voltage $V_{sd} = 0$) versus gate voltage, V_g, and magnetic field, B. Regions shown dark blue have low conductance, and correspond to the regimes of Coulomb blockade for $N = 3$ to 10. In contrast to previous experiments[9–12] on the Kondo effect, all performed on lateral quantum dots with unknown electron number, here the number of confined electrons is precisely known. Red stripes in Fig 2d represent Coulomb peaks as high as $\sim e^2/h$. The B-dependence of the first two lower stripes reflects the ground-state evolution for $N = 3$ and 4. Their similar B-evolution indicates that the third and fourth electron occupy the same orbital state with opposite spin, which is observed also for $N = 1$ and 2 (not shown). This is not the case for $N = 5$ and 6. The $N = 5$ state has $S = 1/2$, and the corresponding stripe shows a smooth evolution with B. Instead, the stripe for $N = 6$ has a kink at $B \approx 0.22$ T. From earlier analyses[24] and from measurements of the excitation spectrum at finite V_{sd} (discussed below), we can identify this kink with a transition in the ground state from a spin triplet to a spin singlet. At the triplet–singlet transition (at $B = B_0$ in Fig. 2c) we observe a strong enhancement of the conductance. In fact, over a narrow range around 0.22 T, the Coulomb gap for $N = 6$ disappears completely.

To explore this conductance anomaly, we show in Fig. 3a differential conductance measurements, dI/dV_{sd} versus V_{sd}, taken at $B = B_0$ and V_g corresponding to the dotted line in Fig. 2d. At temperature $T = 14$ mK, the narrow resonance around zero bias has a full-width at half-maximum, FWHM, of ~ 30 μV. This is several times smaller than the lifetime broadening, $\Gamma = \Gamma_R + \Gamma_L \approx 150$ μV, estimated from the FWHM of the Coulomb peaks. The height of the zero-bias resonance decreases logarithmically with T (Fig. 3b). These are typical 'fingerprints' of the Kondo effect. From FWHM $\approx k_B T_K$, we estimate $T_K \approx 350$ mK. We note that we can safely neglect the Zeeman spin splitting because $g\mu_B B_0 \approx 5\,\mu\text{V} \ll k_B T_K$, implying that the spin triplet is in fact three-fold degenerate at $B = B_0$. This condition is essential to the Kondo effect illustrated in Fig. 1b. Alternative schemes have recently been proposed for a Kondo effect where the degeneracy of the triplet state is lifted by a large magnetic field[25,26].

For $N = 6$, we find markedly anomalous T-dependence only at the

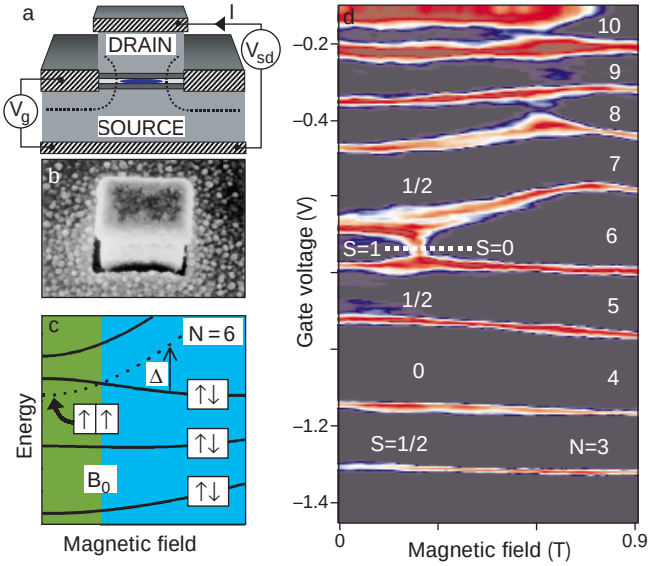

Figure 2 Sample description, energy spectrum and magnetic-field evolution of the ground state. **a**, Cross-section of our rectangular quantum dot. The semiconductor material consists of an undoped AlGaAs(7 nm)/InGaAs(12 nm)/AlGaAs(7 nm) double barrier structure sandwiched between n-doped GaAs source and drain electrodes. A gate electrode surrounds the pillar and is used to control the electrostatic confinement in the quantum dot. A d.c. bias voltage, V_{sd}, is applied between source and drain, and current, I, flows vertically through the pillar. In addition to V_{sd}, we apply a modulation with r.m.s. amplitude $V_{ac} = 3$ μV at 17.7 Hz for lock-in detection. The gate voltage, V_g, can change the number of confined electrons, N, one-by-one from ~ 10 at $V_g = 0$ to 0 at $V_g = -1.8$ V. A magnetic field, B, is applied along the vertical axis. Temperature, T, is varied between 14 mK and 1 K. Our lowest effective electron temperature is 25 ± 5 mK. **b**, Scanning electron micrograph of a quantum dot with dimensions $0.45 \times 0.6\ \mu\text{m}^2$ and height of ~ 0.5 μm. **c**, Schematic energy spectrum. Solid lines represent the B-evolution of the first four orbital levels in a single-particle model. The dashed line is obtained by subtracting the two-electron exchange coupling from the fourth level. At the crossing between this dashed line and the third orbital level at $B = B_0$ the ground state for $N = 6$ undergoes a triplet-to-singlet transition. $B_0 \approx 0.22$ T with a slight dependence on V_g. We define Δ as the energy difference between the triplet and the singlet states. **d**, Colour-scale representation of the linear conductance versus V_g and B. Red stripes denote conductance peaks of height $\sim e^2/h$. Blue regions of low conductance indicate Coulomb blockade. The V_g-position of the stripes reflects the ground-state evolution with B, for $N = 3$ to 10. The $N = 6$ ground state undergoes a triplet-to-singlet transition at $B_0 \approx 0.22$ T, which results in a conductance anomaly inside the corresponding Coulomb gap.

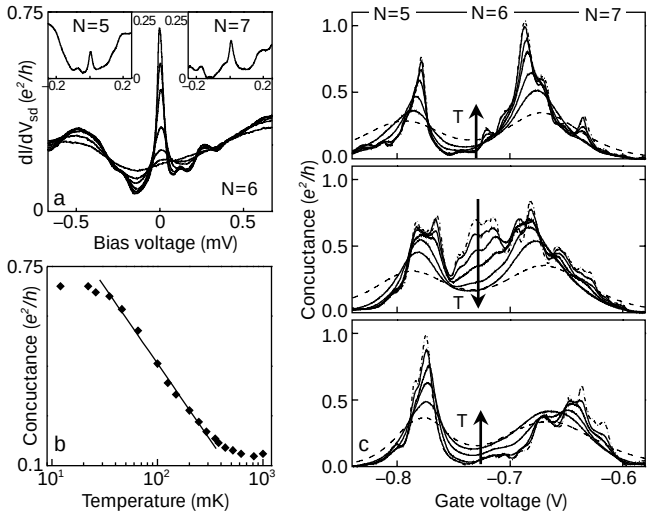

Figure 3 Zero-bias resonance and T-dependence of the conductance at the singlet–triplet degeneracy. **a,** Kondo resonance at the singlet–triplet transition. The dI/dV_{sd} versus V_{sd} curves are taken at $V_g = -0.72$ V, $B = 0.21$ T and for $T = 14$, 65, 100, 200, 350, 520 and 810 mK. Insets to **a**: Kondo resonances for $N = 5$ (left inset) and $N = 7$ (right inset), measured at $V_g = -0.835$ V and $V_g = -0.625$ V, respectively, and for $B = 0.11$ T and $T = 14$ mK. **b**, Peak height of zero-bias Kondo resonance versus T as obtained from **a** (filled diamonds). The line demonstrates a logarithmic T-dependence, which is characteristic of the Kondo effect. The saturation at low T is probably due to electronic noise. **c**, T-dependence of the linear conductance versus V_g for $B = 0.12$ T (spin-triplet ground state), $B = 0.22$ T (singlet–triplet degeneracy), and $B = 0.32$ T (spin-singlet ground state). Each panel shows 7 traces at $T = 20$ (dot-dashed line), 35, 70, 120, 260, 490 (solid lines) and 1,050 (dashed line) mK. The arrows emphasize the temperature dependence in the valley for $N = 6$.

singlet–triplet degeneracy. Figure 3c shows the conductance versus V_g for different T. The upper panel shows data for $B = 0.12$ T. The two Coulomb peaks correspond to the transition from $N = 5$ to 6 and from $N = 6$ to 7. The small, short-period modulations superimposed on the Coulomb peaks are due to a weak charging effect in the upper part of the GaAs pillar above the dot[27]. We will ignore this fine structure and focus on the general T-dependence. Upon increasing T, the valley conductance for $N = 6$ goes up due to thermally activated transport. A similar behaviour is seen in the lower graph for $B = 0.32$ T. In contrast, at the singlet–triplet transition for $B = 0.22$ T we find an opposite T-dependence, again indicating the formation of a Kondo resonance. At the lowest T, the valley conductance is as high as $0.7e^2/h$, which is close to the height of the Coulomb peaks.

The T-dependence for $N = 5$ and 7 is visibly different from that in the non-Kondo valley for $N = 6$ (lower panel of Fig. 3c). Such a difference is a manifestation of the ordinary spin-1/2 Kondo effect expected for odd N. Indeed the corresponding zero-bias resonances are clearly observed (see insets to Fig. 3a). Their height, however, is much smaller than for the singlet–triplet Kondo effect. There is also some indication for a triplet Kondo effect in the T-dependence for $N = 6$ at $B = 0.12$ T, although the associated zero-bias anomaly is not as apparent.

We now investigate the effect of lifting the singlet–triplet degeneracy by changing B at a fixed V_g corresponding to the dotted line in Fig. 2d. Near the edges of this line, that is, away from B_0, the Coulomb gap is well developed, as denoted by the dark colours in Fig. 2d. The dI/dV_{sd} versus V_{sd} traces still exhibit anomalies, however, now at finite V_{sd} (see Fig. 4a). For $B = 0.21$ T we observe the singlet–triplet Kondo resonance at $V_{sd} = 0$. At higher B, this resonance splits apart showing two peaks at finite V_{sd}. It is important to note that these peaks occur inside the Coulomb gap. They result from "inelastic" co-tunnelling events[16,28], where "inelastic" refers to energy exchanging between quantum dot and electrodes (see right drawing in Fig. 4d). The upper traces in Fig. 4a, for $B < 0.21$ T, also show peak structures, although less pronounced.

In Fig. 4b we plot the positions of the dI/dV_{sd} peaks in the plane of V_{sd} and B. The different symbols refer to different gate voltages, and it can be seen that these positions do not depend on V_g. The solid lines are obtained from the excitation spectrum measured (see Fig. 4c) in direct tunnelling (see left-hand drawing in Fig. 4d). They represent the measured B-dependence of the singlet–triplet energy difference, Δ. The fact that these independent measurements coincide implies that inelastic co-tunnelling occurs when $eV_{sd} = \pm\Delta$. Note that this condition is independent of V_g, consistent with our observations. We believe that for small Δ ($\lesssim k_B T_K$), the split resonance reflects the singlet–triplet Kondo anomaly shifted to finite bias. This resembles the splitting of the Kondo resonance by the Zeeman effect[9,10,29], although on a very different B-scale. In the present case, the splitting occurs between two different multiparticle states and originates from the B-dependence of the orbital motion. For increasing Δ, the shift to larger V_{sd} induces spin-decoherence processes, which broaden and suppress the finite-bias peaks[29]. For $B \approx 0.39$ T the peaks have evolved into steps[28], which may indicate that the spin-coherence associated with the Kondo effect has completely vanished. □

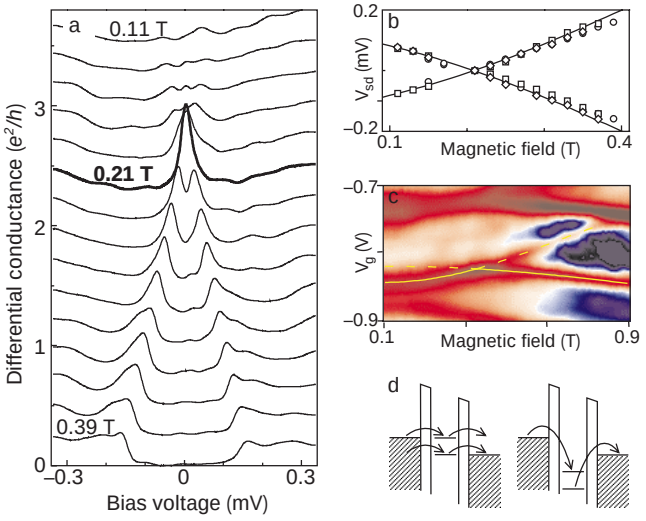

Figure 4 Singlet–triplet energy separation tuned by a magnetic field. **a**, dI/dV_{sd} versus V_{sd} characteristics taken along the dotted line in Fig. 2d ($V_g = -0.72$ V) at equally spaced magnetic fields $B = 0.11, 0.13, \ldots, 0.39$ T. Curves are offset by 0.25 e^2/h. **b,** Extracted peak positions from dI/dV_{sd} curves in **a** versus B. Each symbol refers to a gate voltage taken between −0.72 and −0.70 V. **c**, Colour-scale plot of dI/dV_{sd} measured at $V_{sd} = 0.67$ mV as a function of B and V_g. The solid line identifies the ground state, whereas the dashed line indicates the first excited state[8] for $N = 6$. From their difference we extract the singlet–triplet energy splitting, $\Delta(B)$, using a proportionality factor $\alpha = 6.7$ meV V^{-1} to convert gate voltage into energy. The two solid lines in **b** represent $\pm\Delta(B)$ with a horizontal shift of 0.08 T to compensate for the shift of the singlet–triplet transition to a higher magnetic field in a high-bias measurement. **d**, Energy diagrams for two different transport regimes, both with $eV_{sd} = \Delta$. Left: both ground and excited states lie between the two Fermi energies, so two channels are available for direct tunnelling. The excitation spectrum in **c** is measured in this regime. Right: both ground and excited states lie below the Fermi levels of the leads (Coulomb blockade regime). Inelastic co-tunnelling is illustrated, where one electron tunnels out of the lower-energy state and another tunnels into the higher-energy state.

Received 3 February; accepted 28 April 2000.

1. Hewson, A. C. *The Kondo Problem to Heavy Fermions* (Cambridge University Press, 1993).
2. Cox, D. L. & Maple, M. B. Electronic pairing in exotic superconductors. *Phys. Today* **48,** 32–40 (1995).
3. Prinz, G. A. Magnetoelectronics. *Science* **282,** 1660–1663 (1998).
4. Loss, D. & DiVincenzo, D. P. Quantum computation with quantum dots. *Phys. Rev. A* **57,** 120–126 (1998).
5. Madhavan, V., Chen, W., Jamneala, T., Crommie, M. F. & Wingreen, N. S. Tunneling into a single magnetic atom: spectroscopic evidence of the Kondo resonance. *Science* **280,** 567–569 (1998).
6. Li, J., Schneider, W.-D., Berndt, R. & Delley, B. Kondo scattering observed at a single magnetic impurity. *Phys. Rev. Lett.* **80,** 2893–2896 (1998).
7. Awschalom, D. D. & DiVincenzo, D. P. Complex dynamics of mesoscopic magnets. *Phys. Today* **48,** 43–48 (1995).
8. Tarucha, S., Austing, D. G., Tokura, Y., van der Wiel, W. G. & Kouwenhoven, L. P. Direct Coulomb and exchange interaction in artificial atoms. *Phys. Rev. Lett.* **84,** 2485–2488 (2000).
9. Goldhaber-Gordon, D. *et al.* Kondo effect in a single-electron transistor. *Nature* **391,** 156–159 (1998).
10. Cronenwett, S. M., Oosterkamp, T. H. & Kouwenhoven, L. P. A tunable Kondo effect in quantum dots. *Science* **281,** 540–544 (1998).
11. Schmid, J., Weis, J., Eberl, K. & von Klitzing, K. A quantum dot in the limit of strong coupling to reservoirs. *Physica B* **256–258,** 182–185 (1998).
12. Simmel, F., Blick, R. H., Kotthaus, J. P., Wegsheider, W. & Bichler, M. Anomalous Kondo effect in a quantum dot at nonzero bias. *Phys. Rev. Lett.* **83,** 804–807 (1999).
13. Kouwenhoven, L. P. *et al.* in *Mesoscopic Electron Transport* (eds Sohn, L. L., Kouwenhoven, L. P. & Schön, G.) 105–214 (NATO ASI Ser. E 345, Kluwer, Dordrecht, 1997).
14. Glazman, L. I. & Raikh, M. E. Resonant Kondo transparency of a barrier with quasilocal impurity states. *JETP Lett.* **47,** 452–455 (1988).
15. Ng, T. K. & Lee, P. A. On-site Coulomb repulsion and resonant tunneling. *Phys. Rev. Lett.* **61,** 1768–1771 (1988).
16. Averin, D. V. & Nazarov, Y. V. in *Single Charge Tunneling* (eds Grabert, H. & Devoret, M. H.) 217–247 (Proc. NATO ASI Ser. B 294, Plenum, New York, 1991).
17. Mattis, D. C. Symmetry of ground state in a dilute magnetic metal alloy. *Phys. Rev. Lett.* **19,** 1478–1481 (1967).
18. Nozières, P. & Blandin, A. Kondo effect in real metals. *J. Phys.* **41,** 193–211 (1980).
19. Wan, Y., Phillips, P. & Li, Q. Suppression of the Kondo effect in quantum dots by even-odd asymmetry. *Phys. Rev. B* **51,** 14782–14785 (1995).
20. Izumida, W., Sakai, O. & Shimizu, Y. Kondo effect in single quantum dot systems—study with NRG method. *J. Phys. Soc. Jpn* **67,** 2444–2454 (1998).
21. Maurer, S. M., Patel, S. R., Marcus, C. M., Duruöz, C. I. & Harris, J. S. Jr Coulomb blockade fluctuations in strongly coupled quantum dots. *Phys. Rev. Lett.* **83,** 1403–1406 (1999).
22. Schmid, J., Weis J., Eberl, K. & von Klitzing, K. Absence of odd-even parity behaviour for Kondo resonances in quantum dots. *Phys. Rev. Lett.* (submitted).
23. Eto, M. & Nazarov, Yu. V. Enhancement of Kondo effect in quantum dots with even number of electrons. Preprint cond-mat/0002010 (cited 29 May 2000) at ⟨http:xxx.lanl.gov⟩ (2000).
24. Austing, D. G. *et al.* Ellipsoidal deformation of vertical quantum dots. *Phys. Rev. B* **60,** 11514–11523 (1999).
25. Pustilnik, M., Avishai, Y. & Kikoin, K. Quantum dots with even number of electrons: Kondo effect in a finite magnetic field. *Phys. Rev. Lett.* **84,** 1756–1759 (2000).
26. Giuliano, D. & Tagliacozzo, A. Spin fractionalization of an even number of electrons in a quantum dot. *Phys. Rev. Lett.* **84,** 4677–4680 (2000).
27. Sivan, U. *et al.* Spectroscopy, electron-electron interaction, and levels in a disordered quantum dot. *Europhys. Lett.* **25,** 605–611 (1994).

28. Funabashi, Y., Ohtsubo, K., Eto, M. & Kawamura, K. Phase relaxation and non-equilibrium transport properties through multilevel quantum dot. *Jpn J. Appl. Phys.* **38,** 388–391 (1999).
29. Wingreen, N. S. & Meir, Y. Anderson model out of equilibrium: Noncrossing-approximation approach to transport through a quantum dot. *Phys. Rev. B* **49,** 11040–11052 (1994).
30. Inoshita, T., Shimizu, A., Kuramoto, Y. & Sakaki, H. Correlated electron transport through a quantum dot: The multiple-level effect. *Phys. Rev. B* **48,** 14725–14728 (1993).

Acknowledgements

We thank Yu. V. Nazarov, K. Maijala, S. M. Cronenwett, J. E. Mooij and Y. Tokura for discussions. We acknowledge financial support from the Specially Promoted Research, Grant-in-Aid for Scientific Research, from the Ministry of Education, Science and Culture in Japan, from the Dutch Organisation for Fundamental Research on Matter (FOM), from the NEDO joint research program, and from the EU via a TMR network.

Correspondence and requests for materials should be addressed to S.D.F. (e-mail: silvano@qt.tn.tudelft.nl).

Direct observation of the alignment of ferromagnetic spins by antiferromagnetic spins

F. Nolting*, A. Scholl*, J. Stöhr†, J. W. Seo‡§, J. Fompeyrine§, H. Siegwart§, J.-P. Locquet§, S. Anders*, J. Lüning†, E. E. Fullerton†, M. F. Toney†, M. R. Scheinfein‖ & H. A. Padmore*

* *Advanced Light Source, 1 Cyclotron Road, Lawrence Berkeley National Laboratory, Berkeley, California 94720, USA*
† *IBM Research Division, Almaden Research Center, 650 Harry Road, San Jose, California 95120, USA*
‡ *Institute de Physique, University of Neuchâtel, CH-2000 Neuchâtel, Switzerland*
§ *IBM Research Division, Zürich Research Laboratory, CH-8803 Rüschlikon, Switzerland*
‖ *Department of Physics and Astronomy, Arizona State University, Tempe, Arizona 85287-1504, USA*

The arrangement of spins at interfaces in a layered magnetic material often has an important effect on the properties of the material. One example of this is the directional coupling between the spins in an antiferromagnet and those in an adjacent ferromagnet, an effect first discovered[1] in 1956 and referred to as exchange bias. Because of its technological importance for the development of advanced devices such as magnetic read heads[2] and magnetic memory cells[3], this phenomenon has received much attention[4,5]. Despite extensive studies, however, exchange bias is still poorly understood, largely due to the lack of techniques capable of providing detailed information about the arrangement of magnetic moments near interfaces. Here we present polarization-dependent X-ray magnetic dichroism spectro-microscopy that reveals the micromagnetic structure on both sides of a ferromagnetic–antiferromagnetic interface. Images of thin ferromagnetic Co films grown on antiferromagnetic $LaFeO_3$ show a direct link between the arrangement of spins in each material. Remanent hysteresis loops, recorded for individual ferromagnetic domains, show a local exchange bias. Our results imply that the alignment of the ferromagnetic spins is determined, domain by domain, by the spin directions in the underlying antiferromagnetic layer.

We investigated a thin Co film on top of a 40 nm $LaFeO_3$ film grown on $SrTiO_3$(001). The sample was prepared in a molecular beam epitaxy system with the $LaFeO_3$ film grown using a block-by-block growth method[6] at 750 °C under a beam of atomic oxygen and a partial O_2 pressure of 5×10^{-6} Torr. This method has been shown to yield high-quality epitaxial films[7]. Plan-view electron-diffraction and conventional transmission electron microscopy (TEM) analysis show that the epitaxial $LaFeO_3$ film consists of two microscopic crystallographic domains characterized by orientations of the $LaFeO_3$ **c**-axis along the [100] and [010] directions in the $SrTiO_3$ surface plane[8]. The Co film, grown in the form of a stepped wedge, was deposited *in situ* at room temperature and capped with a 1-nm Pt layer to prevent its oxidation. X-ray diffraction analysis of a sample with a Co thickness of 2.5 nm (and a 1-nm Pt cap layer) revealed a polycrystalline Co structure. Kerr measurements showed that the easy magnetization axis of the sample was in-plane with uniaxial symmetry about the surface normal. All measurements reported here were performed on as-grown samples. Because the samples were not set in a magnetic field they did not exhibit a macroscopic exchange bias[4,5]. (For $LaFeO_3$, chemical decomposition prevents the use of setting temperatures close to the Néel temperature (740 K) to create large exchange bias. However, low-temperature (390 K) annealing of Co/$LaFeO_3$ in a 500-Oe applied field is sufficient to produce a macroscopic bias of 0.007 erg cm^{-2} at room temperature and 0.1 erg cm^{-2} at 4.2 K). Our ability to probe the spatially resolved magnetic configuration allowed us to observe local bias effects, which average to zero macroscopically.

Spectro-microscopy studies were carried out using the PEEM2 facility at the Advanced Light Source in Berkeley[9]. The focused X-rays, whose polarization could be changed from linear to right or left circular[10], are incident on the sample at an angle of 30° from the surface and form a 30-μm spot. The low-energy secondary photoelectrons from the sample are imaged by an all-electrostatic photoemission electron microscope (PEEM) with magnification onto a phosphor screen that is read by charge-coupled device (CCD) camera. The spatial resolution of PEEM2 is limited by chromatic aberrations to 20 nm. For imaging we exploited several unique spectroscopic capabilities associated with the variable energy and polarization of the X-rays[10]. By tuning the photon energy to either the Fe L-edge, near 710 eV, or the Co L-edge, near 780 eV, we can record separate images of the antiferromagnetic (AFM) $LaFeO_3$ layer and the ferromagnetic (FM) Co layer. We use linear X-ray

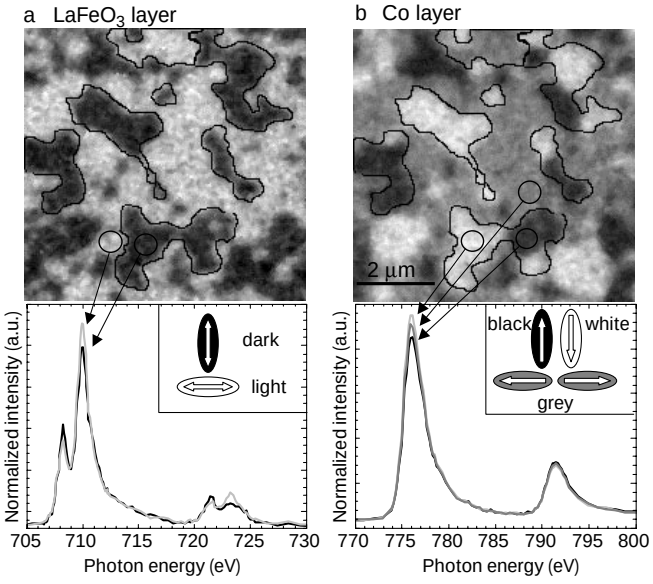

Figure 1 Images and local spectra from the antiferromagnetic and ferromagnetic layers for 1.2-nm Co on $LaFeO_3/SrTiO_3$(001). **a**, Fe L-edge XMLD image; **b**, Co L-edge XMCD image. The contrast in the images arises from antiferromagnetic domains in $LaFeO_3$ (**a**) and ferromagnetic domains in Co (**b**) with in-plane orientations of the antiferromagnetic axis and ferromagnetic spins as indicated below the images. The spectra shown underneath were recorded in the indicated areas and illustrate the origin of the intensity contrast in the PEEM images.